Soil Dynamics and Earthquake Engineering 30 (2010) 1089–1105

Contents lists available at ScienceDirect

Soil Dynamics and Earthquake Engineering

journal homepage: www.elsevier.com/locate/soildyn

Seismic performance of bar-mat reinforced-soil retaining wall: Shaking table testing versus numerical analysis with modified kinematic hardening constitutive model

I. Anastasopoulos *, T. Georgarakos, V. Georgiannou, V. Drosos, R. Kourkoulis

National Technical University of Athens, Greece

ARTICLE INFO

Article history:
Received 18 November 2009
Received in revised form
14 April 2010
Accepted 17 April 2010

Keywords:
Reinforced soil
Shaking Table Testing
Numerical Analysis
Constitutive Relations
Experimental Calibration Data
Scale Effects

ABSTRACT

Reinforced-soil retaining structures possess inherent flexibility, and are believed to be insensitive to earthquake shaking. In fact, several such structures have successfully survived destructive earthquakes (Northridge 1994, Kobe 1995, Kocaeli 1999, and Chi-Chi 1999). This paper investigates *experimentally and theoretically* the seismic performance of a typical bar-mat retaining wall. First, a series of reduced-scale shaking table tests are conducted, using a variety of seismic excitations (real records and artificial multi-cycle motions). Then, the problem is analyzed numerically employing the finite element method. A modified kinematic hardening constitutive model is developed and encoded in ABAQUS through a user-defined subroutine. After calibrating the model parameters through laboratory element testing, the retaining walls are analyzed *at model scale*, assuming model parameters appropriate for very *small confining pressures*. After validating the numerical analysis through comparisons with shaking table test results, the problem is re-analyzed *at prototype scale* assuming model parameters for *standard confining pressures*. The results of shaking table testing are thus *indirectly* "converted" (extrapolated) to real scale. It is shown that: (a) for medium intensity motions (typical of $M_s \approx 6$ earthquakes) the response is "*quasi-elastic*", and the permanent lateral displacement in reality could not exceed a few centimeters; (b) for larger intensity motions (typical of $M_s \approx 6.5$–7 earthquakes) bearing the effects of forward rupture directivity or having a large number of strong motion cycles, plastic deformation accumulates and the permanent displacement is of the order of 10–15 cm (at prototype scale); and (c) a large number of strong motion cycles ($N > 30$) of *unrealistically* large amplitude ($A = 1.0$ g) is required to activate a failure wedge behind the region of reinforced soil. Overall, the performance of the bar-mat reinforced-soil walls investigated in this paper is totally acceptable for realistic levels of seismic excitation.

1. Introduction

Invented by the French Architect and Engineer Henri Vidal in the late 50s, "*reinforced earth*" can be characterized as a composite material. It combines the compressive and shear strength of a thoroughly compacted "select" granular fill (with specific requirements concerning grain distribution, fines content, plasticity index, friction angle, etc.) with the tensile strength of reinforcing materials, such as mild steel (e.g. dip galvanized flat ribbed strips or welded wire mats) or geosynthetic polymers (polypropylene, polyethylene, or polyester geogrids, or woven and non-woven geo-textiles). The latter compensates for the weak strength of soil in tension, rendering reinforced earth the direct analog of reinforced concrete in soil. Depending on the nature of the reinforcement, a reinforced earth system may be characterized as inextensible (when the reinforcement fails without stretching as much as the soil) or extensible (when the opposite is true). Inextensible steel reinforcements are most common for critical structures, such as bridge abutments where control of deformation is crucial. On the other hand, extensible geosynthetic reinforcement is often used in reinforced slopes, basal reinforcement, and temporary retaining walls, where there is no concern for displacement.

Reinforced earth retaining walls posses a number of technical and economic advantages compared to standard gravity walls: (a) they can be constructed rapidly, without requiring large construction equipment; (b) they require less site preparation and less space in front of the structure for construction operations, thus reducing the cost of right-of-way acquisition; (c) they do not need rigid foundation support as they are tolerant to deformations; and (d) they are very cost effective and technically feasible even for heights exceeding 25 m. The first such wall in a seismically active area was constructed in California's Sate Highway 39, in 1972. Since then, in recognition of all the

* Corresponding author.
E-mail address: ianast@civil.ntua.gr (I. Anastasopoulos).

0267-7261/$ - see front matter © 2010 Elsevier Ltd. All rights reserved.
doi:10.1016/j.soildyn.2010.04.020

previously discussed advantages, their use quickly spread universally in highway, industrial, military, commercial, and residential applications.

Reinforced earth structures have all the necessary "ingredients" to be earthquake resistant: being flexible, they tend to follow the dynamic deformation of the retained (free-field) soil without attracting substantially large dynamic earth pressures (e.g. [1]). Indeed, several reinforced soil walls have experienced large intensity destructive earthquakes (Loma Prieta 1989, Northridge 1994, Kobe 1995, Chi-Chi 1999, and Kocaeli 1999) without considerable damage. One of the most dramatic such examples is the 1994 M_w 6.8 Northridge earthquake. With many recorded PGA values higher than 0.60 g, the inflicted damage to structures of all kinds was rather extensive, while 5 major freeway bridges, 18 parking stations, and 40 buildings totally collapsed. Surprisingly, the damage to 23 reinforced soil walls of several heights within the affected area of the earthquake was minor [2]. Regardless of their location and recorded level of PGA, all of them were found to be fully intact with no conspicuous structural damage. Only in one case, minor concrete spalling on the facing panel was observed.

Even more interesting is the performance of reinforced earth walls during the 1995 M_w 7 Kobe earthquake. With recorded PGAs exceeding 0.8 g, the damage was devastating with the direct economic loss exceeding $100 billion [3–6]. The damage to all sorts of structures was more than devastating: from the Kobe Port which was practically put out of service (all but 7 of its 186 berths were totally damaged) to the spectacular overturning structural collapse of a 630 m section the elevated Hanshin Expressway, to countless collapses of bridges and buildings, and to numerous landsides. Also substantial was the damage to a variety of gravity-type retaining structures [7–10]. In marked contrast, damage to reinforced earth walls was rather minor [11,12]. A total of 124 reinforced earth structures, of height ranging from 2 to 17 m were inspected after the earthquake. Although most of them had been designed for ground acceleration of the order of 0.15 g, 74% of them sustained no damage at all, 24% had only very minor damage (mainly displacement), and only 2% showed some damage to the wall facing and movement of the retained soil. No collapse or clear failure was observed.

The seismic performance of reinforced earth structures has been investigated experimentally with various methods: from soil element testing [13], to centrifuge model testing [14–21], and shaking table testing at reduced [22,23], and at nearly full scale [18,24–26]. Among the several conclusions

(i) the critical acceleration is a function of backfill density [21];
(ii) the stiffness, spacing, and length of the reinforcement directly affect the stability and the lateral and vertical deformation of the wall [15,17–19,21];
(iii) the length of the reinforcement is not crucial, as long as it exceeds 70% of the wall height [21];
(iv) the backfill is subjected to substantial densification and settlement [19,21];
(v) current pseudo-static seismic stability analyses based on the limit equilibrium method underestimate their seismic stability [24,27];
(vi) the largest lateral displacement takes place at the middle-height of the wall [19]; and
(vii) finite element (FE) simulation can capture the dynamic response of reinforced earth walls, provided that nonlinear soil response is modeled with a realistic constitutive law [18,25].

This paper investigates *experimentally* and *analytically* the seismic response of typical reinforced soil (bar-mat) retaining walls. First, we present the experimental setup and the key results of a series of reduced-scale shaking table testing. Then, a nonlinear FE model is developed for the same problem. A modified kinematic hardening model is developed and encoded in ABAQUS through a user subroutine. The parameters are calibrated through experimental data (soil element testing of the "*Longstone*" sand used in the experiments): (a) for small confining pressures (which are considered representative for the 1*g* shaking table tests), and (b) for standard confining pressures (which are considered representative for the prototype problem). First, we analyze the shaking table test (assuming model parameters for small confining pressures) to validate the analysis methodology and the constitutive model. Then, we analyze the prototype (assuming model parameters for standard confining pressures), thus extending our results to the real scale.

2. Shaking table testing

A series of two models were constructed and tested at the Laboratory of Soil Mechanics of the National Technical University of Athens (NTUA), utilizing a recently installed shaking table. The table, 1.3 m $\times$ 1.3 m in dimensions, is capable of shaking specimens of 2 tons at accelerations upto 1.6 g. Synthetic accelerograms, as well as real earthquake records can be simulated. The actuator is equipped with a servo-valve, controlled by an analog inner-loop control system and a digital outer-loop controller; it is capable of producing a stroke of ± 75 mm.

At this point, it is noted that the stress field in the backfill soil cannot be correctly reproduced in reduced-scale shaking table testing, and this is the main advantage of centrifuge testing. Its disadvantage, however, is the crude knowledge of soil properties versus depth in most centrifuge tests. Shaking table testing can be seen as a valid option, provided that the results are interpreted carefully, with due consideration to scale effects and the stress-dependent soil behavior.

2.1. Physical model configuration and construction

As shown in Fig. 1, the prototype refers to two reinforced earth retaining walls, both 7.5 m high, positioned back-to-back at 21.4 m distance, supporting a dry granular backfill. Each wall is reinforced with 13 rows of bar-mat grid, at 0.6 m vertical spacing. Following the key conclusions of earlier studies (see discussion above), each reinforcement row is 0.7*H* long (i.e. 5.12 m in prototype scale). Two types of reinforcemnt were selected: (a) a relatively "flexible" reinforcement grid, consisting of 8 mm bars at 20 cm spacing both in the longitudinal and the transverse direction; and (b) a "stiff" reinforcement grid, consisting of 20 mm bars also at 20 cm spacing. In both cases, the facing panels are made of reinforced concrete, 0.2 m in thickness, and 0.6 m in height.

Taking account of the capacity of the shaking table, a $N=20$ scale factor was selected for the experiments, resulting to a total height of the model of 49.8 cm. The selection of model materials was conducted taking account of scaling laws [28], as synopsized in Table 1, so that the simulation is as realistic as posible for the given prototype. The bar-mats were constructed using commercially available steel wire mesh: $d=0.4$ mm at 12 mm spacing, for the "flexible" reinforcement; $d=1$ mm, also at 12 mm spacing, for the "stiff" reinforcement. Athough the stiffness is not accurately scaled, this selection was made as a compromise between the target stiffness and the scaling in terms of the soil-reinforcement interface (which depends on geometry). The facing panels were made of $t=2$ mm plexiglass strips ($E \approx 3$ GPa), and were connected to each other through a customized

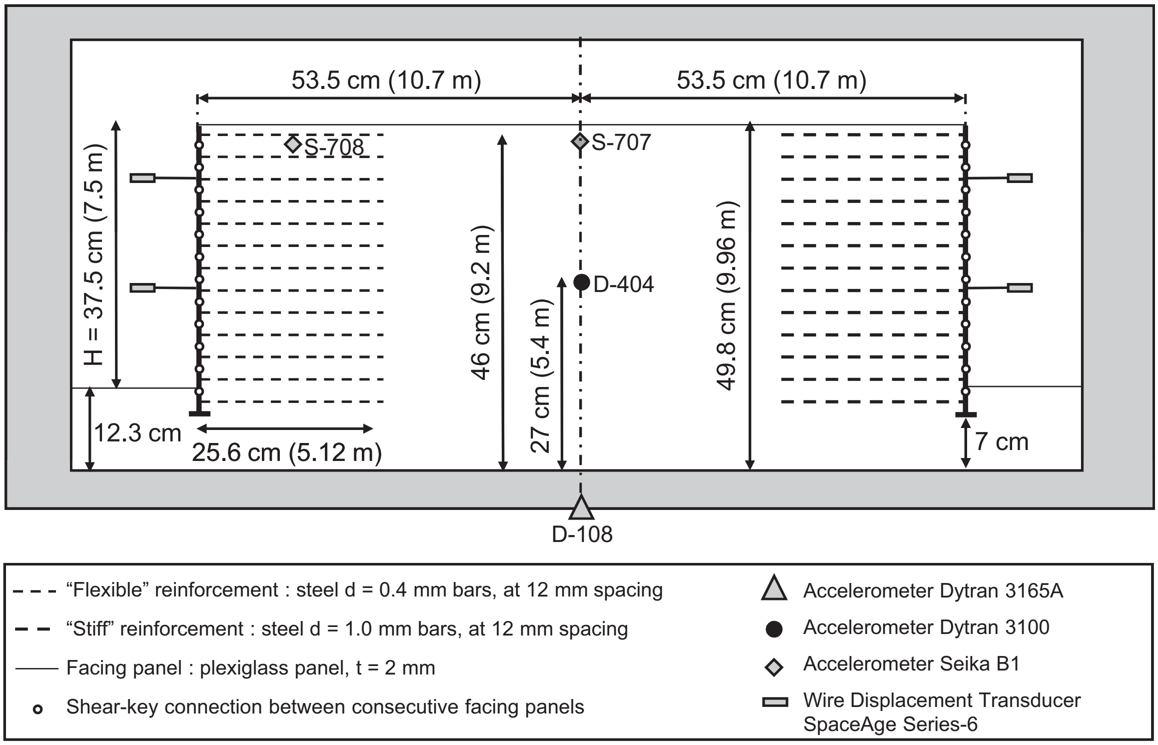

Fig. 1. Shaking table model setup, showing geometry and instrumentation. The models were constructed at 1:20 scale, taking account of the capabilities of the shaking table. The dimensions are given in model scale (prototype scale in parentheses).

Table 1
Scaling factors for 1g and centrifuge modeling (after [28])

Quantity to be scaled	1g scaling factor prototype to model ratio	Centrifuge scaling factor prototype to model ratio
Displacement	N	N
Time (dynamic)	$N^{0.5}$	N
Velocity	$N^{0.5}$	1
Acceleration	1	N^{-1}
Force	ρ^*N^3	N^2
Energy, moment	ρ^*N^4	N^3
Moment of inertia	N^5	N^4
Frequency	$N^{-0.5}$	N^{-1}

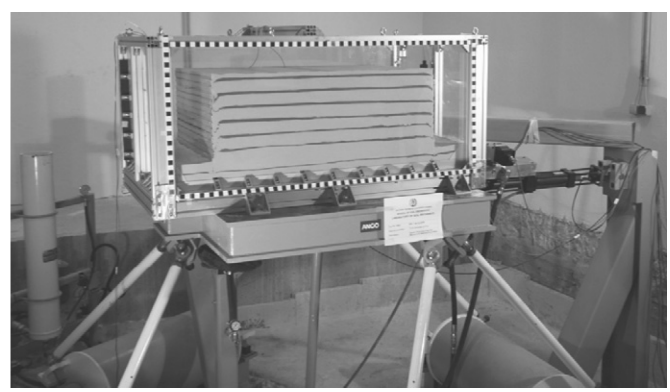

Fig. 2. Reinforced earth retaining wall models (Model-1) inside the rigid sandbox, installed on the NTUA shaking table. The sandbox consists of an aluminum space frame, covered with 16 mm plexiglass panels to allow observation of the deformed specimen.

connection, using a ‘‘shear key’’ configuration to block realtive horizontal dispacemnts between consecutive pannels, but allowing differential rotation (as in reality).

The retaining wall models were placed inside a rigid $160\times 90\times 75$ cm (length × width × height) sandbox (Fig. 2). The latter consists of an alluminum space frame (ASF), covered with 15 mm plexiglass panels to allow observation of the deformed specimen. Static and dynamic finite element anaysis of the box, showed that the whole system is stiff enough to sustain the static (i.e. geostatic) and dynamic (due to shaking) loads of the specimen. The intial design consisted of 10 mm side windows, but eigen-frequency analysis showed that the first dynamic mode was 45 Hz. Thus, the thickness of the side plexiglass panels was increased to 15 mm, so that the dominant mode of the box (at 80 Hz) does not possibly interfere with the shaking modes of the model. A 6 mm glass protection layer is installed inside the plexiglass windows, to protect them from getting scratched from the (quartz) sand particles.

The model is prepared following the real construction sequence of such walls: after placement of a soil layer, the corresponing reinforcement row is installed, followed by the next soil layer, and the next reinforcement, until reaching the top. After placing two succesive soil layers and the corresponding reinforcements, and before proceeding to the next, blue coloured sand is poured close to the window of the sandbox to allow observation of the deformation. A total of 40 stages were required to complete a single model, including sensor installation.

2.2. Backfill preparation and physical properties

The backfill consisted of dry ‘‘Longstone’’ sand, a very fine and uniform quartz sand with $D_{50}=0.15$ mm and uniformity coefficient $D_{60}/D_{10}=1.42$, industrially produced with adequate quality control. The grain size distribution curve for the sand is shown in Fig. 3. The void ratios at the loosest and densest state were

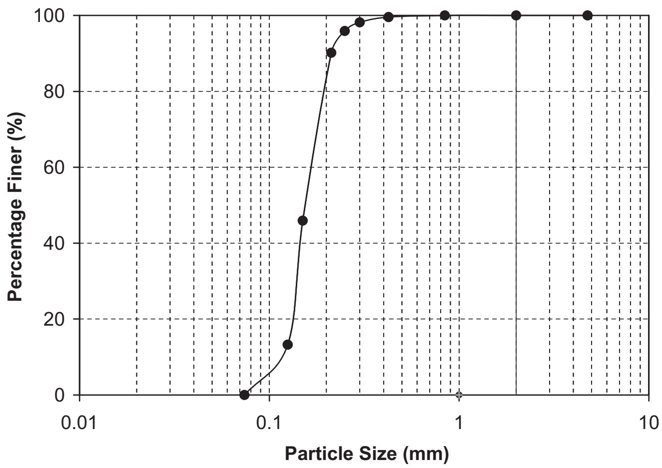

Fig. 3. Grain size distribution of the "Longstone" sand used in the shaking table tests—a fine uniform sand with d_{50}=0.15 mm and uniformity coefficient C_u=1.42.

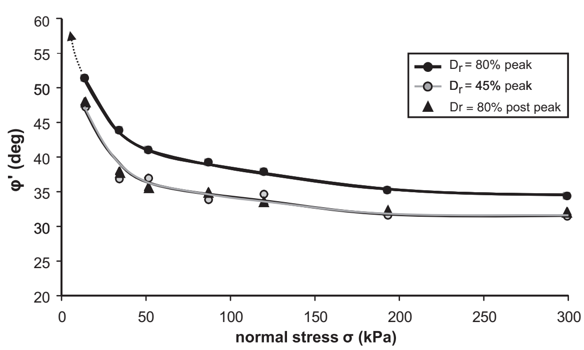

Fig. 4. Direct shear test results: dependence of the angle of shearing resistance on stress level.

measured in the laboratory. Following the procedure described by Kolbuszewski [29] e_{max}=0.995, while e_{min}=0.614, and G_s=2.64.

Direct shear tests were carried out to define peak and post-peak strength characteristics of the sand. Tests were performed on medium loose D_r=45 ± 0.02% and dense specimens D_r=80 ± 0.07% and for a normal stress range from 13 kPa (due to the weight of the top cap only) to 300 kPa. The low normal stress is more representative of the stress level prevailing in the shaking table tests. Loose specimens were prepared by raining the sand into the box while dense specimens were obtained by tapping the box after raining. The loose specimens have shown critical state behavior. The angle of shearing resistance appears to depend strongly on stress level and for stresses higher than 120 kPa $\varphi' \approx 32^\circ$, while for stress levels lower than 100 kPa φ' increases up to 47° at normal stress σ=13 kPa as shown in Fig. 4. For the dense specimens the angle of shearing resistance increases to $\varphi' \approx 35^\circ$ for higher stress levels and to 51° at the lowest normal stress. These values drop after displacement of 6 mm to post-peak values similar to the peak strength of the medium-loose specimens (Fig. 4), indicating an angle of dilation $\psi \approx 6^\circ$.

Taking account of the above, the first test model (Model-1) was constructed with $D_r \approx 44\%$ (to represent the loose state), while the second test model (Model-2) with $D_r \approx 83\%$ (dense state).

Torsional shear tests were also performed in the hollow cylinder apparatus of the National Technical University of Athens [30] to obtain the stress–strain and stiffness characteristics of Longstone sand. Tests were performed keeping the same internal and external pressure (p_i=p_o). Such a condition results in the parameter expressing the influence of the intermediate principal stress, b=($\sigma_2-\sigma_3/\sigma_1-\sigma_3$)=$\sin^2\alpha$, where α is the rotation of principal stress direction from the vertical. The axial load was kept close to zero during the tests and torsional loading was applied under stress control. Tests were controlled and interpreted in terms of average stresses and strains according to the equations, suggested by Hight et al. [31]. Stiffness was expressed in terms of secant ("effective") shear modulus.

In Fig. 5 the effective stress paths under undrained monotonic torsional loading are shown for specimens of Longstone sand tested in the hollow cylinder apparatus. Medium-loose specimens were prepared by pluviation through water [31] and denser specimens by tapping the mould after the sand had settled. The medium loose specimens were isotropically consolidated to mean effective stresses (50, 100, 200, 300 kPa) and their relative densities before shearing, varied between 39.2% and 40.7%.

The resulting curves of excess pore water pressure against shear strain and stress–strain are shown in Fig. 5b and c, respectively. Two denser specimens of Longstone sand shown as light gray lines in the figures will be referred to later. Initially, the medium-loose specimens of Longstone sand show contractive tendencies while shear stress, $\tau_{\theta z}$, and excess pore water pressure, Δu, steadily increase up to the phase transformation points (φ'_{PTL}=36°) marked by the solid arrows in Fig. 5c. Thereafter, all specimens show a tendency to dilate and follow the failure envelope of the sand (φ'_{PTL}=41°, Fig. 5a). It should be noted that the medium-loose specimen consolidated at the lowest confining pressure of 50 kPa appears to follow a failure envelope that corresponds to a mobilized angle of shearing resistance higher than φ'_{PTL}=41° as observed earlier in the shear box tests. The response of two denser specimens (with D_r=45.7% and 47.9%) is also presented in Fig. 5. Contractive tendencies are smaller, but not eliminated. However, the phase transformation line appears to be unique and independent of initial density. On the other hand, the mobilized angle of shearing resistance seems to be higher for the denser specimens (φ'_{dense}=43° versus φ'=41°).

In Fig. 6 the stiffness characteristics under monotonic torsional loading are presented for the medium-loose and denser specimens of Longstone sand. The stiffness data given in the figure have been normalized with respect to the mean effective stress of the medium loose specimens after consolidation, p_c'= 100 kPa. At first, under undrained torsional loading stiffness values are higher for the denser specimens, by about 8%, when compared with the medium-loose ones. This trend remains the same for shear strains $\gamma_{\theta z}$ up to 0.1%. However, with further straining the stiffness curves merge in a single curve and at $\gamma_{\theta z}$=1% the normalized shear modulus is vanishing small.

The shaking table models were prepared by raining the sand from a specific height with controllable mass flow rate (which controls the density of the sand), using a custom raining system (Fig. 7a). As depicted in Fig. 7b, for the maximum raining velocity and the current width of container opening the Longstone sand achieves relative densities D_r ranging from about 10–85%. Observe that beyond a critical height (65–75 cm), the D_r of the specimen is insensitive to the height of raining.

2.3. Instrumentation

Four accelerometers and four wire displacement transducers were installed in the models, as illustrated in Fig. 1. The accelerometers (SEIKA B1, and DYTRAN 3165 A) were placed inside the sand specimen during construction at their predetermined positions. The wire displacement transducers (Space Age Series 6) were installed after completion of the model. The body of each transducer was fixed on the rigid walls of the

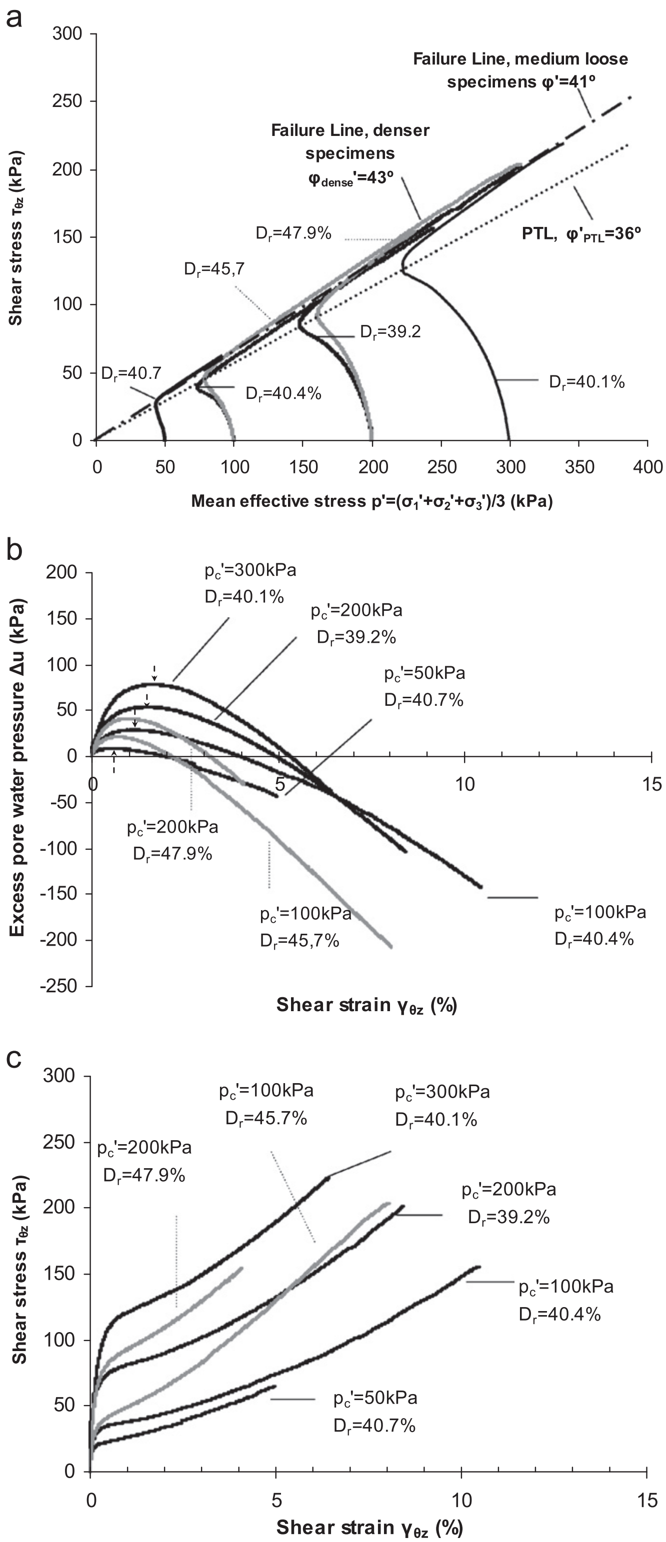

Fig. 5. Monotonic torsional hollow cylinder testing of Longstone sand for a variety of relative densities: (a) effective stress paths; (b) excess pore water pressure versus shear strain; (c) shear stress versus shear strain.

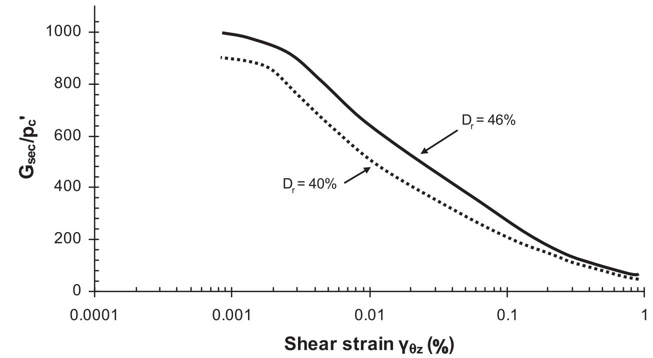

Fig. 6. Effective shear modulus versus shear strain of Longstone sand (measured through monotonic torsional loading).

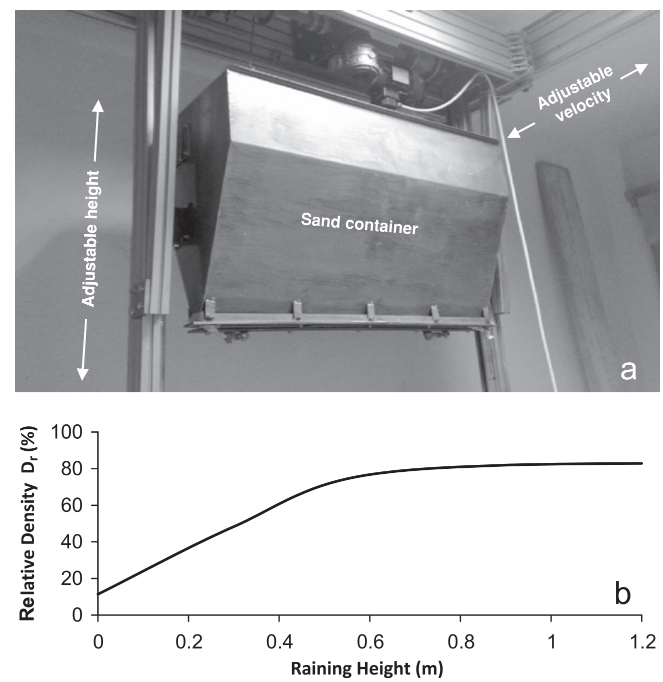

Fig. 7. (a) Electronically controlled sand raining system used for preparation of the models. (b) Relative density D_r with respect to the raining height for a constant velocity.

sandbox, and the sensing wires were connected to the walls of the model through pre-installed anchors. All sensors were connected to the 8-channel data acquisition system of the shaking table.

2.4. Testing sequence and seismic excitation

As summarized in Table 2, two test series were conducted. In the first test series (Model 1), the backfill soil was loose ($D_r \approx 43\%$) and the model was subjected to "extreme seismic shaking": a 60-cycle "cos sweep" of dominant period $T_o = 0.5$ s and $PGA \approx 1.0$ g (Fig. 8). Although not realistic (both in terms of retained soil density *and* shaking intensity), this test was conducted to derive deeper insights on the ultimate capacity of reinforced soil walls.

In the second test series (Model 2), a more realistic case of dense sand ($D_r \approx 85\%$) was subjected to real earthquake records and artificial multi-cycle seismic motions (Figs. 9 and 10). The order of shaking events started with smaller intensity records, followed by the larger ones, and completed with multi-cycle artificial motions: the two 30-cycle so-called "*cos sweeps*" of $PGA = 0.5$ g and $T_o = 0.4$ or 0.8 s. The selected records cover a wide range from medium intensity earthquakes (Lefkada-1973, Kalamata) to stronger seismic events characterized by forward-rupture directivity effects (Rinaldi-228) or large number of significant cycles (Lefkada-2003).

Table 2
Model configuration and shaking sequence of the two shaking table test series.

Model	Backfill	Seismic excitation	Peak acceleration (g)	Dominant period (s)
Model 1	Loose D_r=43%	"Extreme shaking" 60-cycle cos-sweep	1.00	0.50
Model 2	Dense D_r=84%	Lefkada-1973	0.53	0.48
		Kalamata	0.27	0.36
		Lefkada-2003	0.42	0.35
		Rinaldi-228	0.84	0.72
		Cos sweep T=0.4 s	0.50	0.40
		Cos sweep T=0.8 s	0.50	0.80

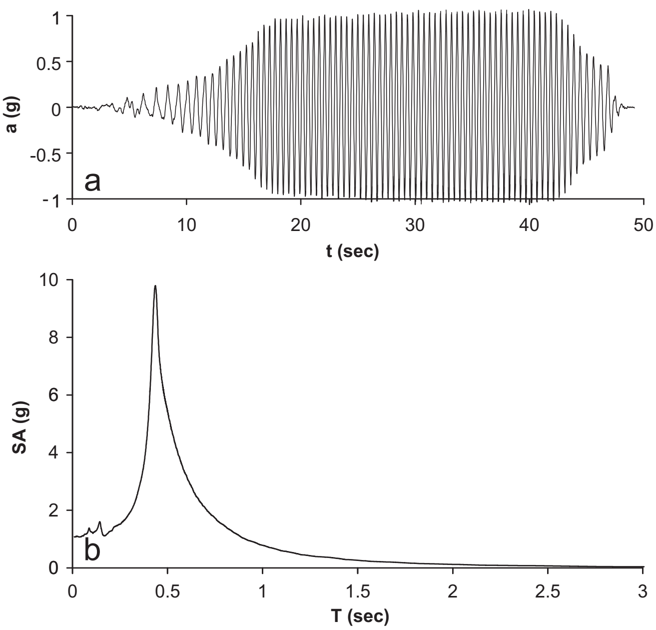

Fig. 8. (a) 60-cycle "extreme shaking" synthetic excitation of the first test (Model 1); and (b) the corresponding elastic acceleration response spectrum.

3. Results of shaking table testing

In the following sections we present the performance of the tested bar-mat reinforced soil walls under extreme seismic shaking and under more realistic seismic motions. As already discussed, an additional substantial difference between the two test series lies in the relative density of the retained soil: loose and dense sand, respectively.

3.1. Performance of loose backfill walls under extreme seismic shaking

The results of the test are shown in terms of characteristic snapshots of the deformed model (Fig. 11), and acceleration and displacement time histories at key model locations (Fig. 12). The response of the reinforced soil wall model can be roughly categorized in three distinct stages:

3.1.1. Stage 1: quasi-elastic response

During the first 11 seconds of the experiment no deformation is conspicuous (Fig. 11), and the response of the system can be described as roughly quasi-elastic. During this stage, the input acceleration has not yet exceeded roughly 0.4 g (Fig. 12), a value which can be seen as the critical acceleration of the reinforced soil walls. In the horizontal displacement histories no substantial deformation is yet observed.

3.1.2. Stage 2: development of active wedge failure

At t=11.72 s a first vertical separation and sliding initiation between the reinforced soil "block" and the backfill can be observed (Fig. 11). The strain localization starts from the top of the backfill moving progressively downwards. At t=12.88 s the two shear lines can be seen to be completely developed, practically reaching the lowest reinforcement row. Just a few seconds later, at t=15.65 s, an active failure wedge starts forming behind the reinforced soil "block". Now, strain localization starts from the bottom (roughly at the depth of the last row of reinforcement), and propagates towards the ground surface. The wedge of the left wall ("flexible" reinforcement) can be seen to propagate towards the surface a bit more rapidly than the one of the right wall ("stiff" reinforcement). At t=18.96 s both shear lines have reached the surface and the active wedges are fully developed. During this stage, appreciable horizontal deformation of the two walls takes place, with the input seismic acceleration reaching 1.0 g (Fig. 12). Interestingly, the measured acceleration at mid-height and at the top of the backfill is substantially lower, implying a rather pronounced de-amplification, something which is attributable to the low stiffness (and strength) of the loose backfill.

3.1.3. Stage 3: accumulation of horizontal deformation and settlement

During this stage, both reinforced soil walls keep accumulating outward horizontal displacement and the (non-reinforced) backfill is subjected to additional densification settlement. Observe that the reinforced soil mass acts indeed as a block, moving outward as a whole with small visible deformation (Fig. 11). As the (extreme) shaking continues relentlessly, the backfill continues to experience dynamic densification (compaction), the sand becomes progressively denser, and the developing acceleration (at mid-height and atop of the wall) exceeds 1.0 g: amplification (Fig. 12). The horizontal (lateral) displacement of the two reinforced soil walls consists of two components: a cyclic (oscillatory) and a permanent (cumulative) component. The first is related to the inertial response of the system, while the latter is the result of accumulation of "sliding" displacement of the reinforced soil mass along with its corresponding active failure wedge.

Comparing now the performance of the two reinforced soil walls, it can be argued that the stiffness of the reinforcement does not play a substantial role (for the cases examined herein): the permanent (residual) displacement of both walls is of the order of 1.2 m (Fig. 12). Notice, however, that in the case of the wall with the "flexible" reinforcement the displacement at mid-height is larger than the one at the top of the wall. This can also be seen clearly in Fig. 11. The cyclic component of the displacement is also somewhat larger compared to the wall with the "stiff" reinforcement. In any case, although some differences do exist, the end result is not sensitive to the stiffness of the reinforcement.

Fig. 13 compares a picture of the shaking table model before and after the end of the test. Both walls have moved outwards in

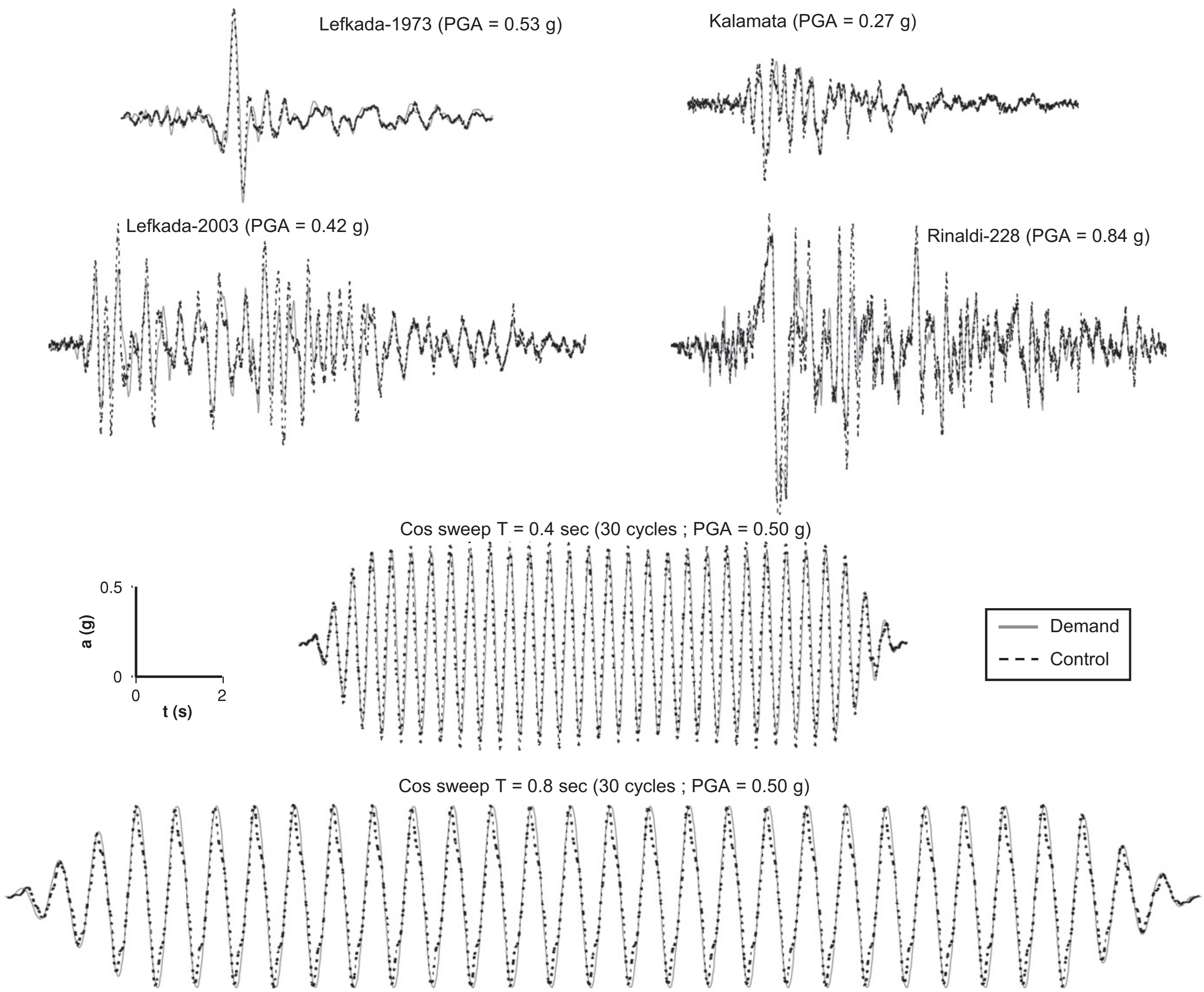

Fig. 9. Real records and artificial multi-cycle accelerograms used as seismic excitations for the second test series (Model 2). The "demand" (i.e. target) time histories are compared with the "control" (i.e. system output) time histories.

the horizontal sense, and the backfill has settled substantially. The latter is due to both, soil densification and horizontal extension of the system. Notice also that the foundation of both walls has rotated substantially.

In summary, despite the large residual deformation, the performance of the two walls under such extreme shaking could be considered acceptable. Both walls exhibited large amounts of ductility, sustaining 60 cycles of 1.0 g input acceleration (and of $T_o = 0.5$ s) without collapsing. Although (as it will be shown later) the soil strength is disproportionally large due to scale effects, such performance is quite remarkable, showing that such systems are quite robust. In fact, this conclusion is in-line with actual earthquake performance of reinforced soil retaining systems. Naturally, this will only be true if the wall is designed to avoid internal failures, such as reinforcement pull-out failure (which depends on the length and spacing of reinforcement), and local failure of one or more facing panels.

3.2. Performance of dense backfill walls under realistic seismic motions

In this section we discuss the results of a more realistic case of dense backfill ($D_r \approx 85\%$) walls subjected to real earthquake records and multi-cycle artificial seismic motions. In stark contrast to the first test series (Model 1), the purpose of which was to intentionally drive the system to failure, in the present test series our aim is to gain insights into the performance of reinforced soil retaining systems under realistically severe conditions. Having thoroughly discussed (see previous section) the failure mechanisms and their evolution with PGA and number of strong motion cycles, we focus herein on the displacement of the walls—a key performance indicator for retaining systems.

3.2.1. Medium intensity earthquakes

The performance is now investigated with two real accelerograms (see also Figs. 9 and 10): (a) the record of the 1973 M_s 6.0 Lefkada (Greece) earthquake [32], and (b) the record of the 1986 M_s 6.2 Kalamata (Greece) earthquake [33]. Both records are from similar magnitude earthquakes and were recorded not far from the causative fault. Also, the inflicted damage to nearby cities (Lefkada and Kalamata, respectively) was substantial.

The recorded time histories of the horizontal displacement Δ are depicted in Fig. 14. In the first case (Lefkada-1973), due to the single acceleration pulse of the input seismic motion, the displacement time history is characterized by a single peak value. As it would be expected, the response of the retaining

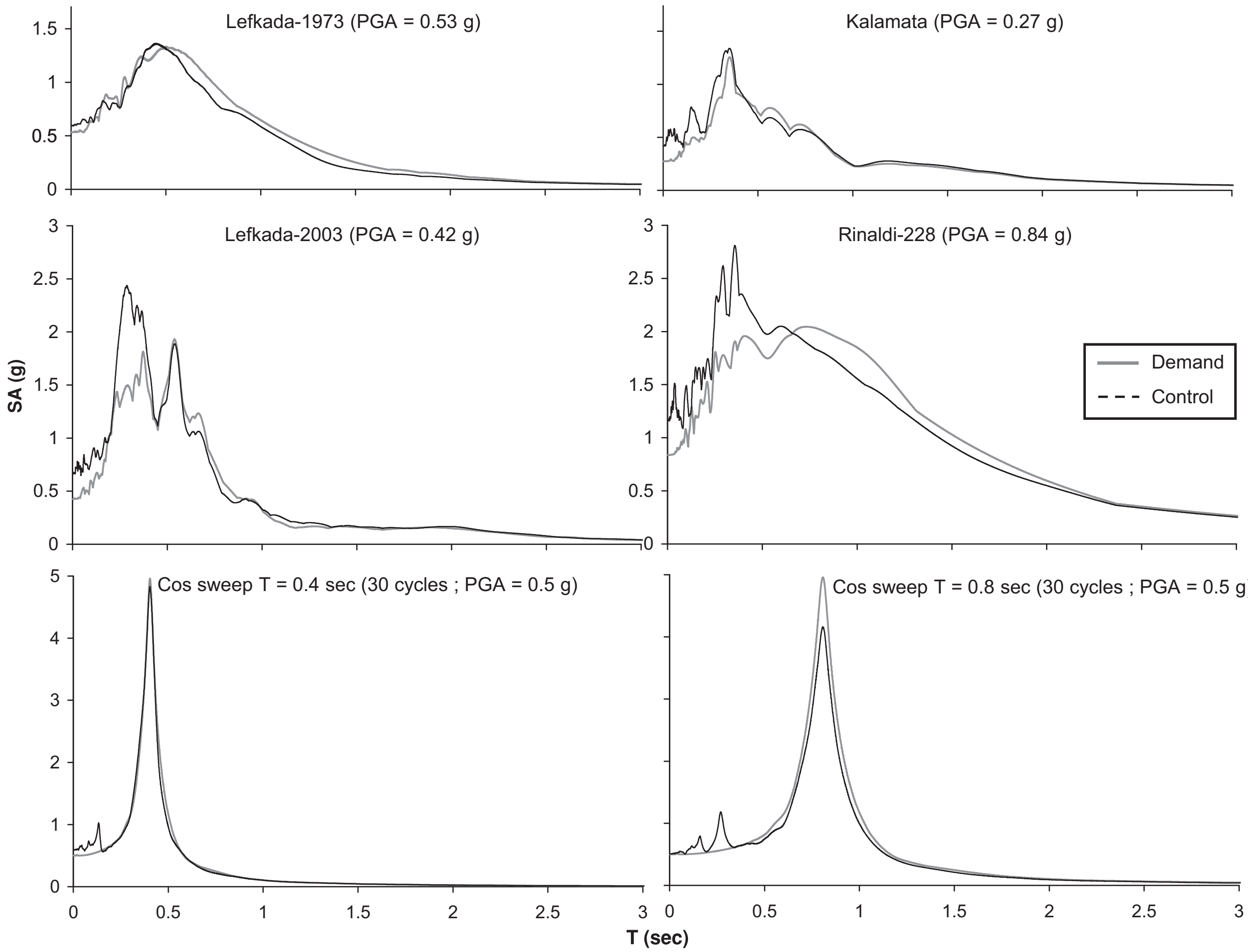

Fig. 10. Elastic response spectra of the real records and synthetic accelerograms used as seismic excitations for the second test series (Model 2). The "demand" (i.e. target) spectra are compared with the "control" (i.e. system output) spectra.

system to the Kalamata seismic motion is dominated by a larger number of peak values, corresponding to the strong motion cycles of the accelerogram. In both cases, the maximum displacement of the wall top is larger than of its mid-height. The residual displacement (in prototype scale) is less than 2 cm for the Lefkada-1973 record and merely exceeds 1 cm for Kalamata. In both cases, the differences between the "stiff" and the "flexible" reinforcement are rather insignificant, and most importantly they are more related to the polarity of shaking (because the two walls are facing to opposite directions) rather than the stiffness of the reinforcement (see also [34–36]).

Summarizing, in view of the damage intensity of both seismic events, a residual (permanent) displacement of 1–2 cm can certainly be characterized as an excellent performance. It is noted, however, that the shaking table experiments were conducted at 1g, and are thus affected by scale effects. This implies (as it will be shown later), that the real permanent displacement may be larger.

3.2.2. Large intensity earthquakes

We now use again two real accelerograms: (a) the record of the 2003 M_s 6.4 Lefkada (Greece) earthquake [37,38], and (b) the Rinaldi (2 2 8) record of the 1994 M_s 6.8 Northridge earthquake [39]. The two records are considered representative of fairly large magnitude earthquakes ($M_s \approx$ 6.5-7.0) and were recorded quite close to the seismogenic fault. The Lefkada-2003 accelerogram was recorded on a medium-soft site at 10 km from the fault, and is characterized by a sequence of roughly eight strong motion cycles, with $PGA = 0.43$ g, $PGV = 33$ cm/s, and a dominant period range 0.3–0.6 s (see also Figs. 9 and 10). Interestingly, the damage to building structures was not pronounced (most of which had been constructed according to traditionally severe seismic requirements), but geotechnical failures were abundant: large-scale landslides, liquefaction and lateral spreading, and most importantly large displacements (of the order of 30 cm or more) of harbor quaywalls. The well-known Rinaldi accelerogram, recorded on stiff soil, is characterized by forward-rupture directivity effects [40].

Fig. 15 depicts the shaking table time histories of retaining wall horizontal displacement Δ. As expected, an accumulation of horizontal displacement can be observed for the Lefkada-2003 record. The peak displacement values reach about 6 cm, with the permanent displacement ranging from 2–4 cm. Interestingly, the largest residual displacement is observed at mid-height of the wall with the "flexible" reinforcement. Although the differences between the "stiff" and the "flexible" reinforcement are partly related to the polarity of the seismic motion, now the stiffness of the bar-mat appears to have played a more substantial role. The response of the two retaining systems is dramatically different for the Rinaldi accelerogram. Now, the acceleration directivity pulse (see Fig. 9) dominates the response, and the displacement time

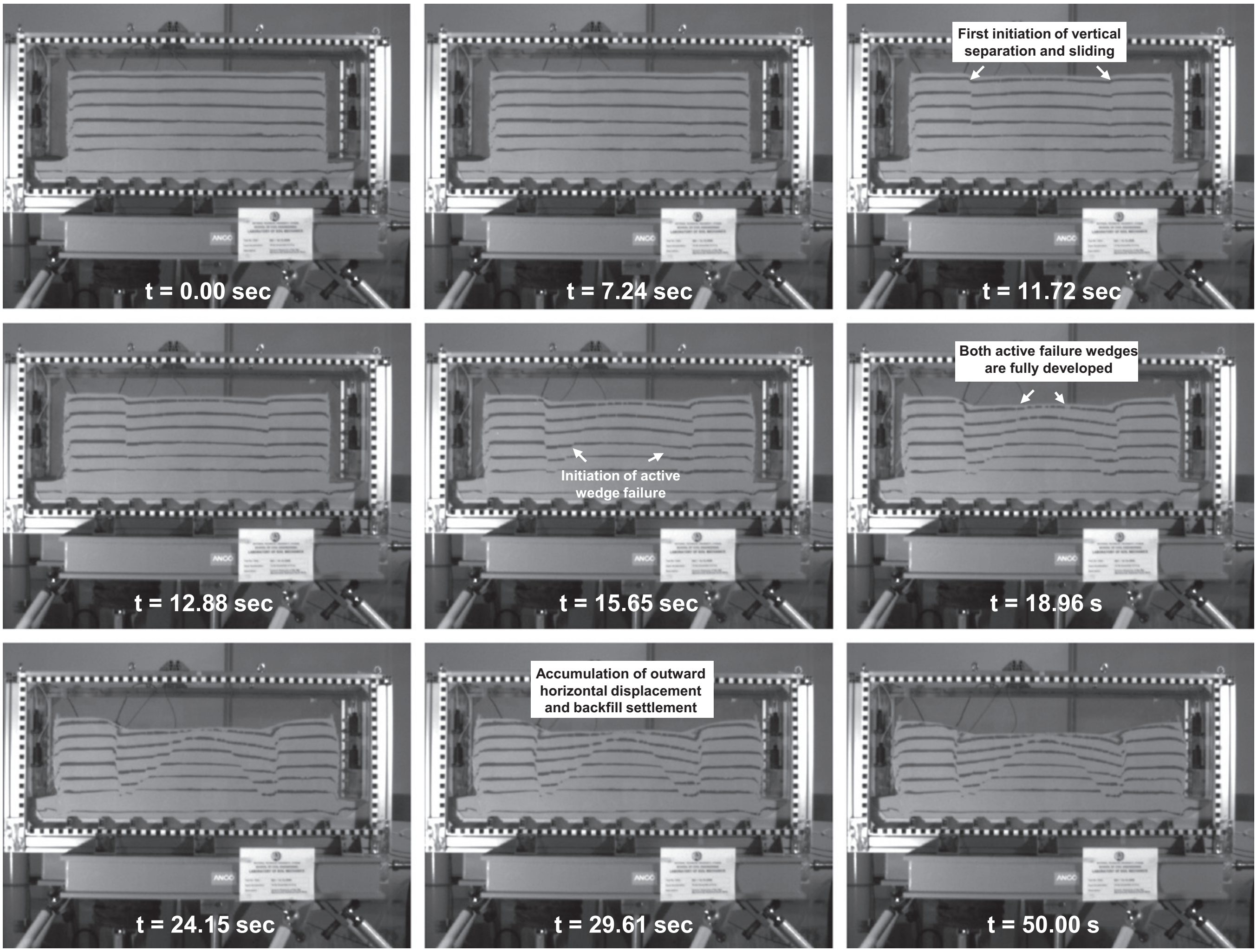

Fig. 11. Shaking table test of retaining walls supporting loose backfill under extreme seismic shaking (Test 1): snapshots of the model at characteristic time intervals (time is shown in prototype scale).

histories are characterized by large peak values of the order of 20 cm (measured at the top). Quite interestingly, the residual (permanent) horizontal displacements do not exceed 10 cm. Notice also that the wall with "flexible" reinforcement is subjected to smaller peak and residual displacements! This paradox is clearly attributable to the polarity of this highly asymmetric seismic motion. For the more flexible system, its orientation was such that the big directivity pulse pushed it inward—a fortuitous (hence unpredictable) occurrence.

In summary, a residual displacement of about 10 cm for such seismic shaking does not only imply survival but can actually be considered as acceptable in terms of strict serviceability requirements. As for the previous cases, scale effects do play a role and the real displacements *will* be larger. But as it will be shown (theoretically) in the sequel, the main conclusion is not qualitatively altered.

3.2.3. Multi-cycle artificial seismic motions

The time histories of horizontal wall displacement Δ for the two artificial 30-cycle cos-sweep motions are illustrated in Fig. 16. As for Model 1, Δ has a cyclic and a cumulative component. In all cases, the cyclic component atop of each wall is substantially larger than at mid-height. Interestingly, the cyclic component at both levels (top and mid-height) and for both walls (with "stiff" and "flexible" reinforcement) is a bit larger for the larger-period ($T_o = 0.8$ s) seismic excitation. With respect to the cyclic component, the stiffness of the reinforcement does not seem to play any measurable role.

In terms of the cumulative component, the differences between the two seismic excitations are not that clear. However, the distribution of Δ is different: while for $T_o = 0.4$ s the difference in Δ between the middle and the top of the wall is rather pronounced (implying an almost linear increase of Δ), for $T_o = 0.8$ s the differences are much less visible (implying a more intense bulging of the wall). Finally, the stiffness of the reinforcement alters the residual displacement of the wall: the maximum residual Δ is 7.5 cm for the wall with "flexible" reinforcement instead of roughly 5 cm for the "stiff" one.

4. Numerical analysis

Two sets of numerical analysis are conducted: (i) analysis of the shaking table model, assuming soil parameters measured for small confining pressures; and (ii) analysis of the prototype, assuming realistic soil parameters for standard confining pressures. The first set of analysis is aimed to corroborate the numerical method and the modified kinematic hardening constitutive soil model. Then, the validated numerical methodology is utilized to predict the actual performance of the prototype. Thus, the results of shaking table testing are indirectly but appropriately "converted" to real scale.

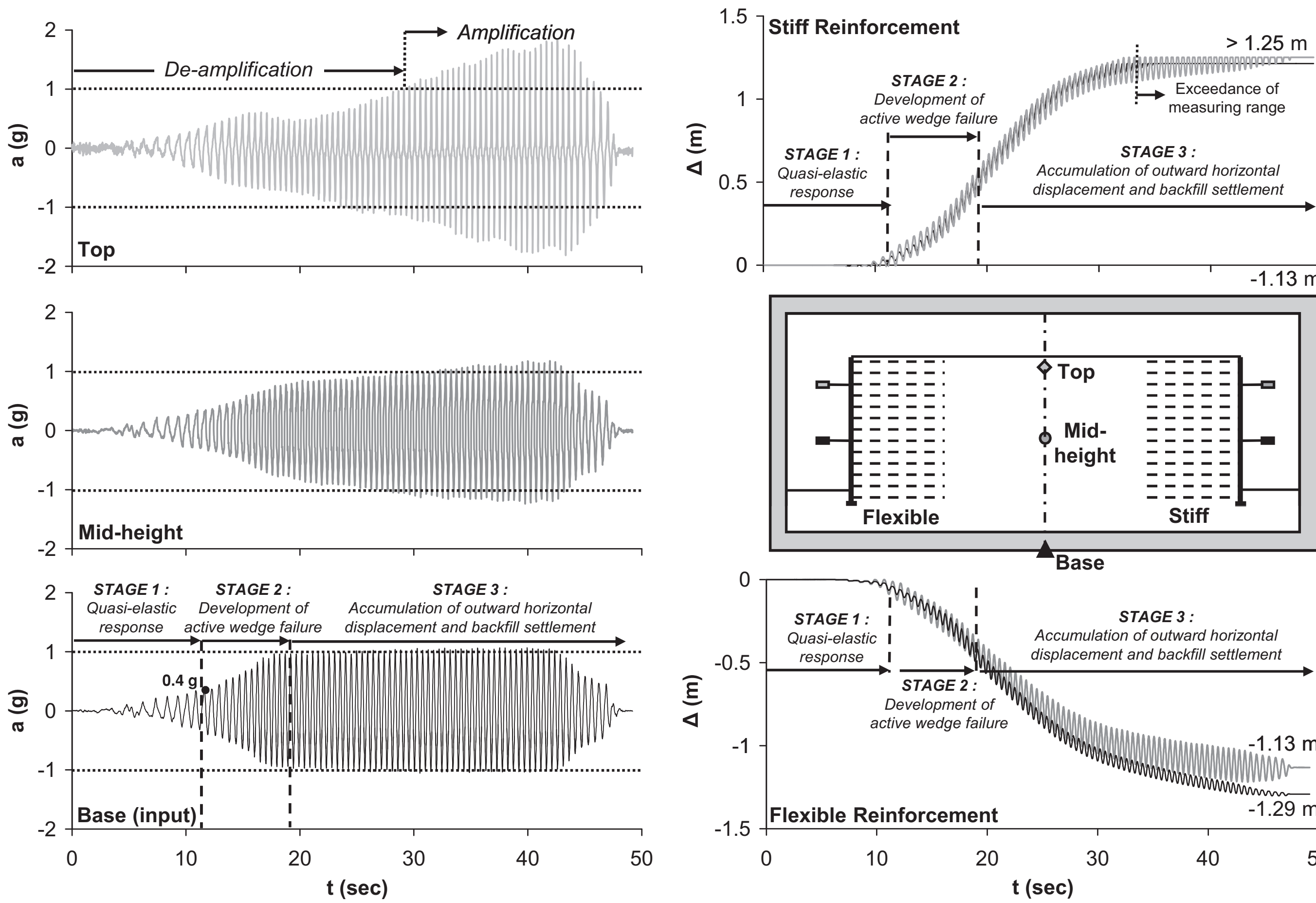

Fig. 12. Shaking table test of retaining walls supporting loose backfill under extreme seismic shaking (Test 1): acceleration time histories at key points, and displacement time histories of the two retaining walls (results shown in prototype scale).

4.1. *Finite element modeling*

Utilizing the finite element code ABAQUS [41], the analysis is conducted assuming plane-strain conditions, and taking account of material and geometric nonlinearities. As schematically illustrated in Fig. 17a, while the soil is modeled with nonlinear continuum elements, elastic beam and truss elements are used for the facing panels and the bar-mat reinforcement, respectively.

Each facing panel consists of two beam elements, and is connected with its neighboring panels with a pinned connection. The latter allows rotation between panels, but restricts the horizontal and vertical degrees of freedom. Thus, the actual shear-key connection between consecutive panels is simulated as realistically as possible. The truss elements simulating the bar-mat reinforcement are assumed to be in perfect contact with soil elements, implying that sliding or pull-out failure cannot take place. Although such a connection may appear to be a gross simplification, it is argued that it is quite realistic for the specific problem: the reinforced walls investigated herein have been designed conservatively to avoid such failures, something which has been verified in all of the conducted experiments.

4.2. *Soil constitutive modeling and calibration against laboratory tests*

The behavior of sand is modeled through a modified kinematic hardening constitutive model. The model combines an extended pressure-dependent Von Mises failure criterion, with nonlinear kinematic hardening and associated plastic flow rule. The evolution of stresses is defined as

$$\sigma = \sigma_0 + \alpha \tag{1}$$

where σ_0 corresponds to the stress at zero plastic strain, and α is the "backstress". The latter is responsible for the kinematic evolution of the yield surface in the stress space. This is performed through a function F which defines the yield surface

$$F = f(\sigma - \alpha) - \sigma_0 \tag{2}$$

Assuming an associated plastic flow rule, the plastic flow rate $\dot{\varepsilon}^{pl}$ is

$$\dot{\varepsilon}^{pl} = \dot{\bar{\varepsilon}}^{pl} \frac{\partial F}{\partial \sigma} \tag{3}$$

where $\dot{\bar{\varepsilon}}^{pl}$ the equivalent plastic strain rate.

The evolution law consists of an isotropic hardening component, which describes the change of the equivalent stress defining the size of the yield surface σ_0 as a function of plastic deformation, and a nonlinear kinematic hardening component. The latter describes the translation of the yield surface in the stress space, and is defined as an additive combination of a purely kinematic term and a relaxation term, which introduces the nonlinearity. The evolution of the kinematic component of the yield stress is described as follows:

$$\dot{\alpha} = C \frac{1}{\sigma_0} (\sigma - \alpha) \dot{\bar{\varepsilon}}^{\rm pl} - \gamma \alpha \dot{\bar{\varepsilon}}^{\rm pl} \tag{4}$$

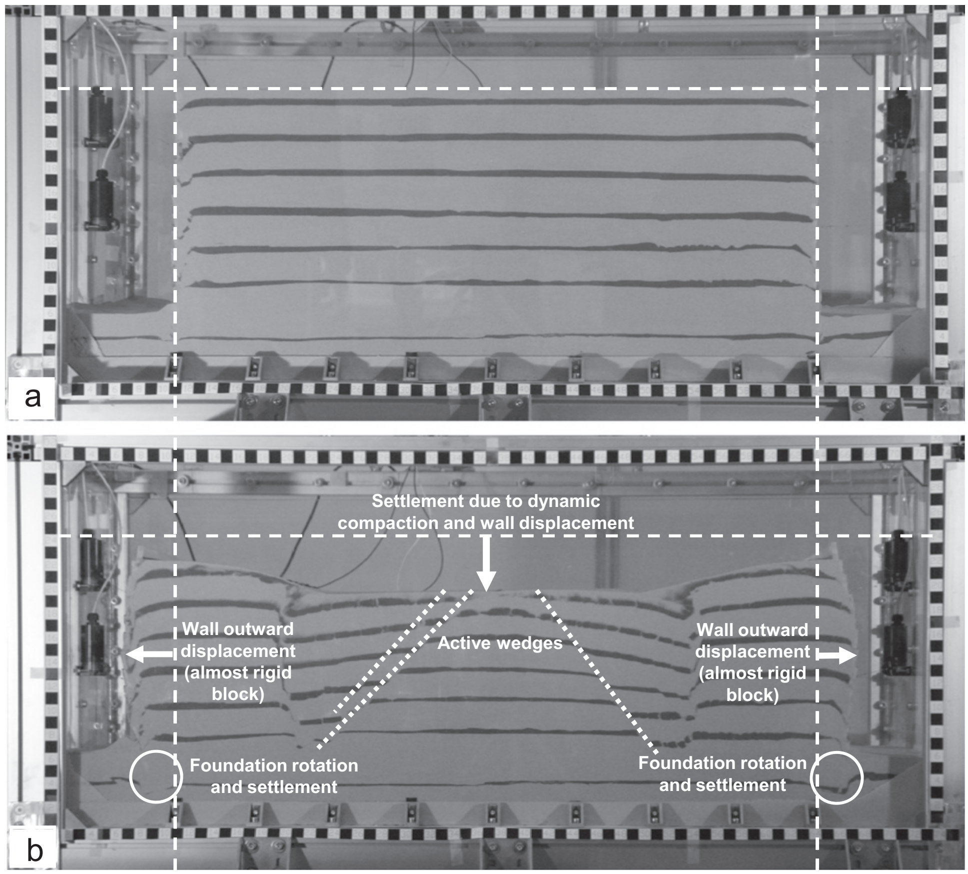

Fig. 13. Shaking table test of retaining walls supporting loose backfill under extreme seismic shaking (Test 1): comparison of (a) physical model before the test, with (b) deformed model after the test.

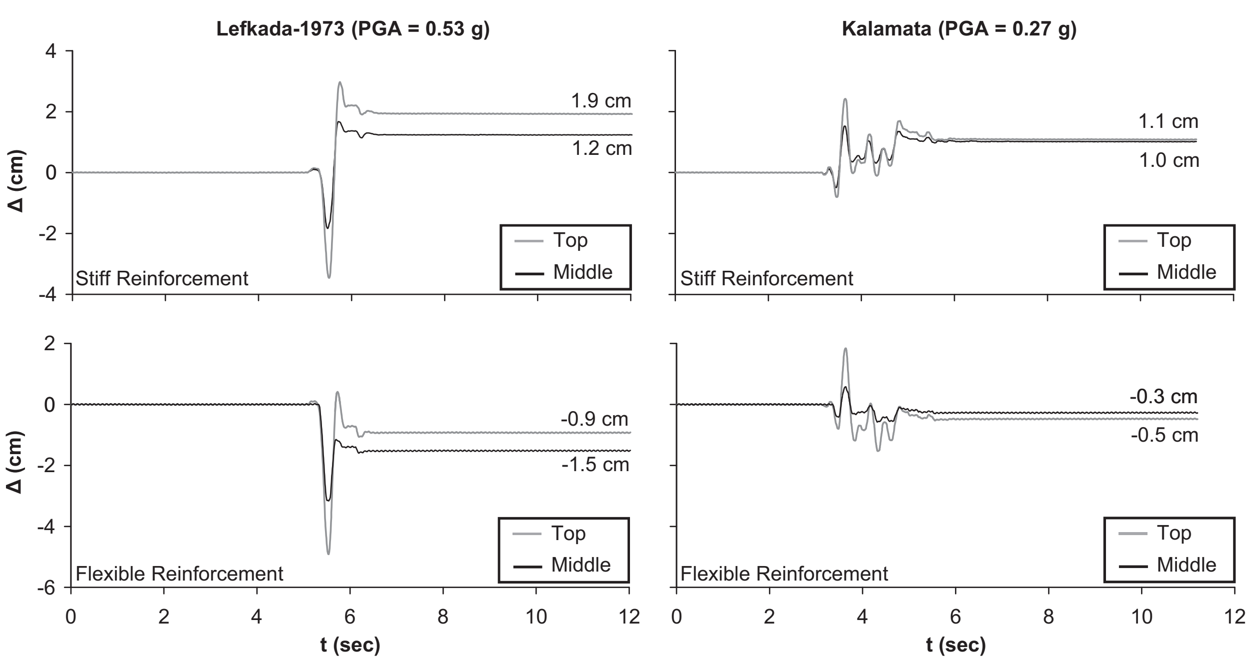

Fig. 14. Shaking table test of retaining walls supporting dense backfill (Test 2): lateral displacement time histories of the two retaining walls for moderate intensity seismic excitation (Lefkada-1973 and Kalamata; results shown in prototype scale).

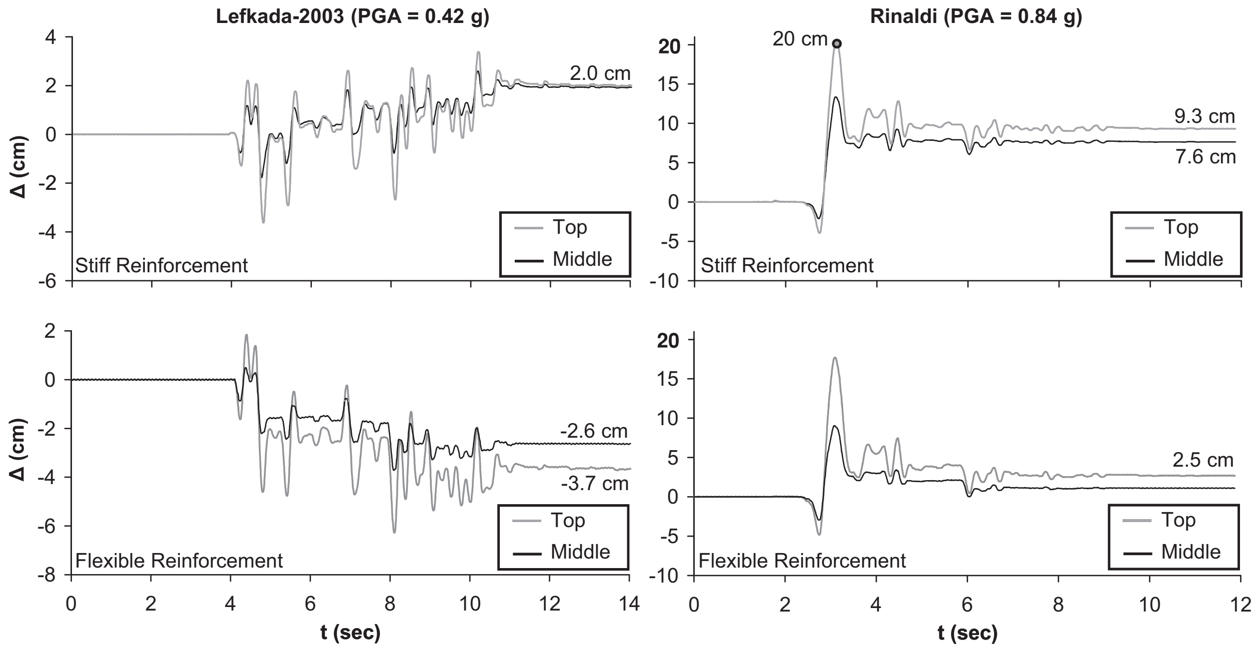

Fig. 15. Shaking table test of retaining walls supporting dense backfill (Test 2): lateral displacement time histories of the two retaining walls for medium and large intensity seismic excitation (Lefkada-2003 and Rinaldi, respectively; results shown in prototype scale).

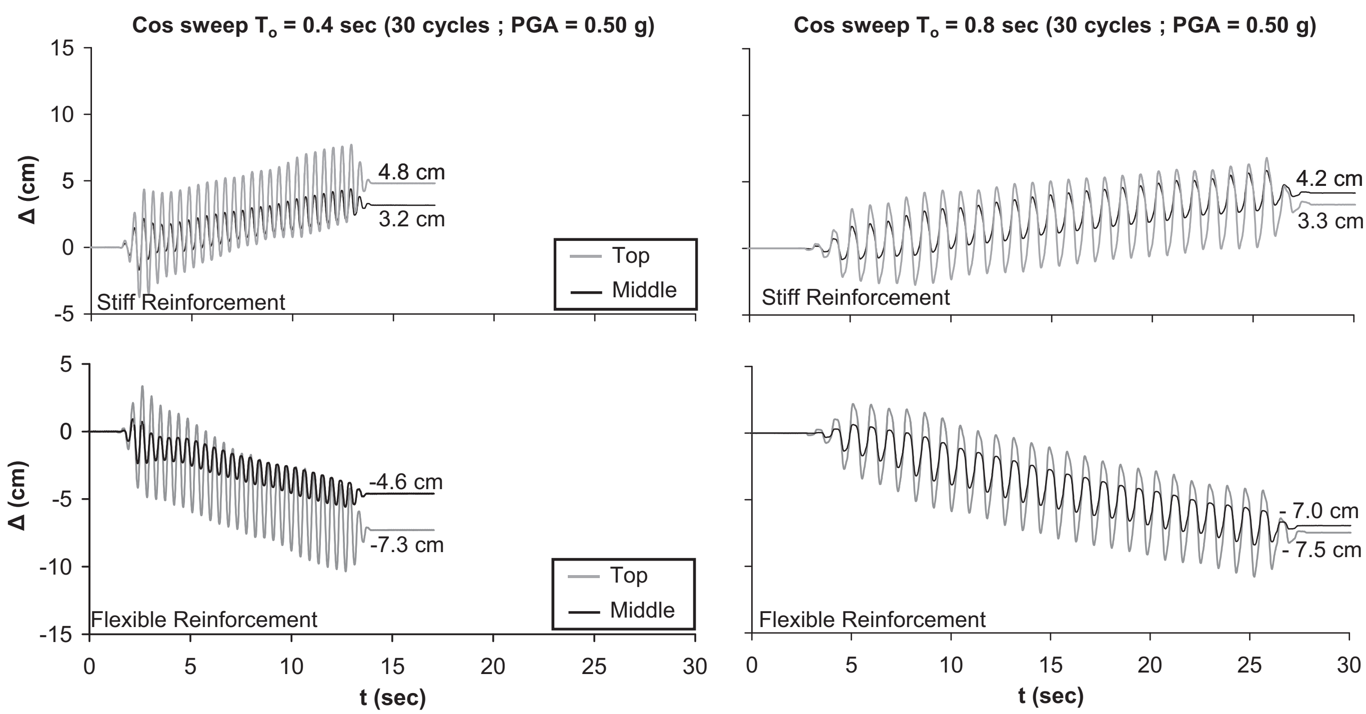

Fig. 16. Shaking table test of retaining walls supporting dense backfill (Test 2): lateral displacement time histories of the two walls for artificial multi-cycle seismic excitations (30-cycle cos sweep T_o=0.4 s, and 0.8 s; results shown in prototype scale).

where C the initial kinematic hardening modulus ($C=\sigma_y/\varepsilon_y=E=2(1+\nu)G_o$) and γ a parameter that determines the rate at which the kinematic hardening decreases with increasing plastic deformation.

The evolution of the two hardening components (kinematic and isotropic) is illustrated in Fig. 17b for unidirectional and multiaxial loading. The evolution law for the kinematic hardening component implies that the backstress α is contained within a cylinder of radius $\sqrt{2/3}C/\gamma$. Since the yield surface remains bounded, this implies that any stress point must lie within a cylinder of radius $\sqrt{2/3}\sigma_y$, where σ_y the maximum yield stress at saturation. To take account of the confining pressure, the latter is defined as a function of the octahedral stress and the friction angle φ of the sand as follows:

$$\sigma_y = \sqrt{3}\left(\frac{\sigma_1+\sigma_2+\sigma_3}{3}\right)\sin\varphi \tag{5}$$

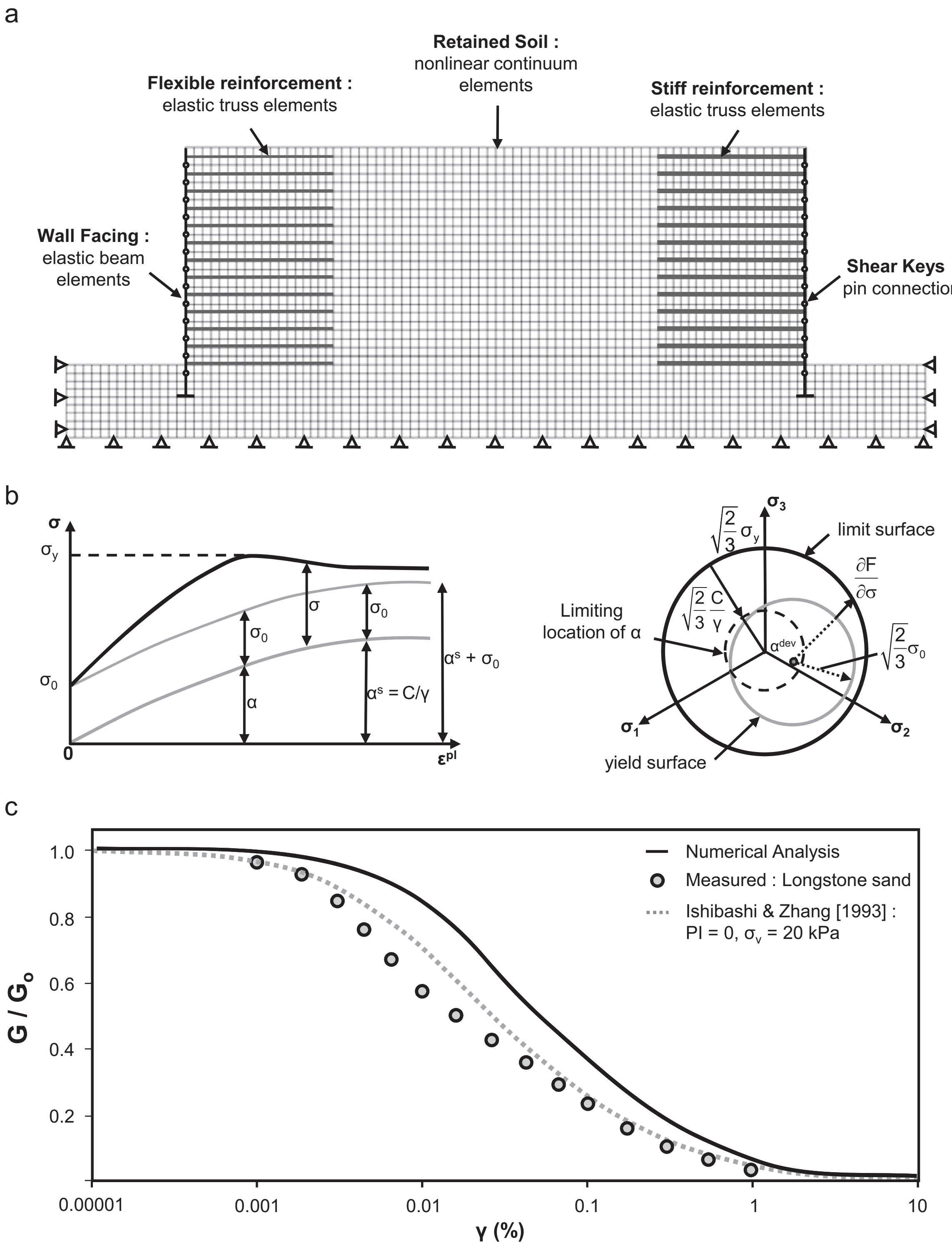

Fig. 17. (a) Overview of the finite element discretization; (b) nonlinear isotropic/kinematic hardening constitutive soil model: simplified onedimensional (left) and three-dimensional (right) representation of the hardening law; (c) calibration of constitutive model against measured and published G:γ curves.

where σ_1,σ_2, and σ_3 the principal stresses. Since $\sigma_y = C/\gamma + \sigma_0$, parameter γ can be written as follows:

$$\gamma = \frac{C}{\sqrt{3}\left(\frac{\sigma_1+\sigma_2+\sigma_3}{3}\right)\sin\varphi - \sigma_0} \qquad (6)$$

The constitutive model is encoded in the ABAQUS [41] finite element environment through a user subroutine. Model parameters are calibrated through experimental data (soil element testing of the sand). Fig. 17c illustrates the validation of the modified kinematic hardening model (through simple shear finite element analysis) against measured (for the "Longstone" sand used in the experiments) and published G–γ curves from the literature [42].

The shear modulus G_o at small strains was estimated on the basis of: (a) bender-element measurements within the shaking table reinforced soil model; (b) the expression of Seed et al. [43]

$$G_o = 1000K_2(\sigma'_m)^{0.5} \qquad (7)$$

where σ'_m the effective mean stress, and K_2 a shear modulus coefficient which is a function of grain size distribution and size, and the relative density; and (c) the expression of Hardin and Richart [44]:

$$G_o = A\frac{(2.973-e)^2}{1+e}(\sigma'_m)^n \tag{8}$$

where A is a parameter similar to K_2 and n a parameter usually taken equal to 0.50.

The angle φ of shearing resistance was estimated on the basis of the laboratory tests (see Figs. 4 and 5). For the analysis of the prototype, we use the measured friction angle for standard confining stresses: $\varphi=38^\circ$. On the other hand, for the analysis of the model, to take account of scale effects (at least to some extent) we have to consider an increased friction angle for very small confining stresses. Going back to the direct shear test results of Fig. 4, observe that for normal stress $\sigma\approx 15$ kPa a friction angle of about 53° was measured. Since the height of our shaking table model is approximately 0.5 m, the "average" effective stress level is of the order of 5 kPa. Hence, "extrapolating" for $\sigma\approx 5$ kPa, a small scale (i.e. at low confining pressures) $\varphi_s\approx 58^\circ$ is derived. It is noted that such a value of small scale φ has been reported in the past for other types of sand (e.g. [45]).

5. Results of numerical analysis and interpretation

The results of the numerical analyses are summarized in Figs. 18 and 19, and Table 3. The results are shown for both sets of analysis (analysis of the shaking table test, assuming model parameters for small confining pressures; and analysis of the prototype, assuming model parameters for standard confining pressures). The first set (analysis of the shaking table model) is compared directly with shaking table test results, to serve as validation of the numerical analysis and of the modified kinematic hardening constitutive model. The second set (analysis of the prototype) is used as an indirect numerical prediction of the actual performance of the prototype.

As depicted in Figs. 18 and 19 the numerical prediction (analysis of shaking table model) compares well with the results of the shaking table tests for the two artificial 30-cycle cos-sweeps. The numerical analysis underestimates the cyclic

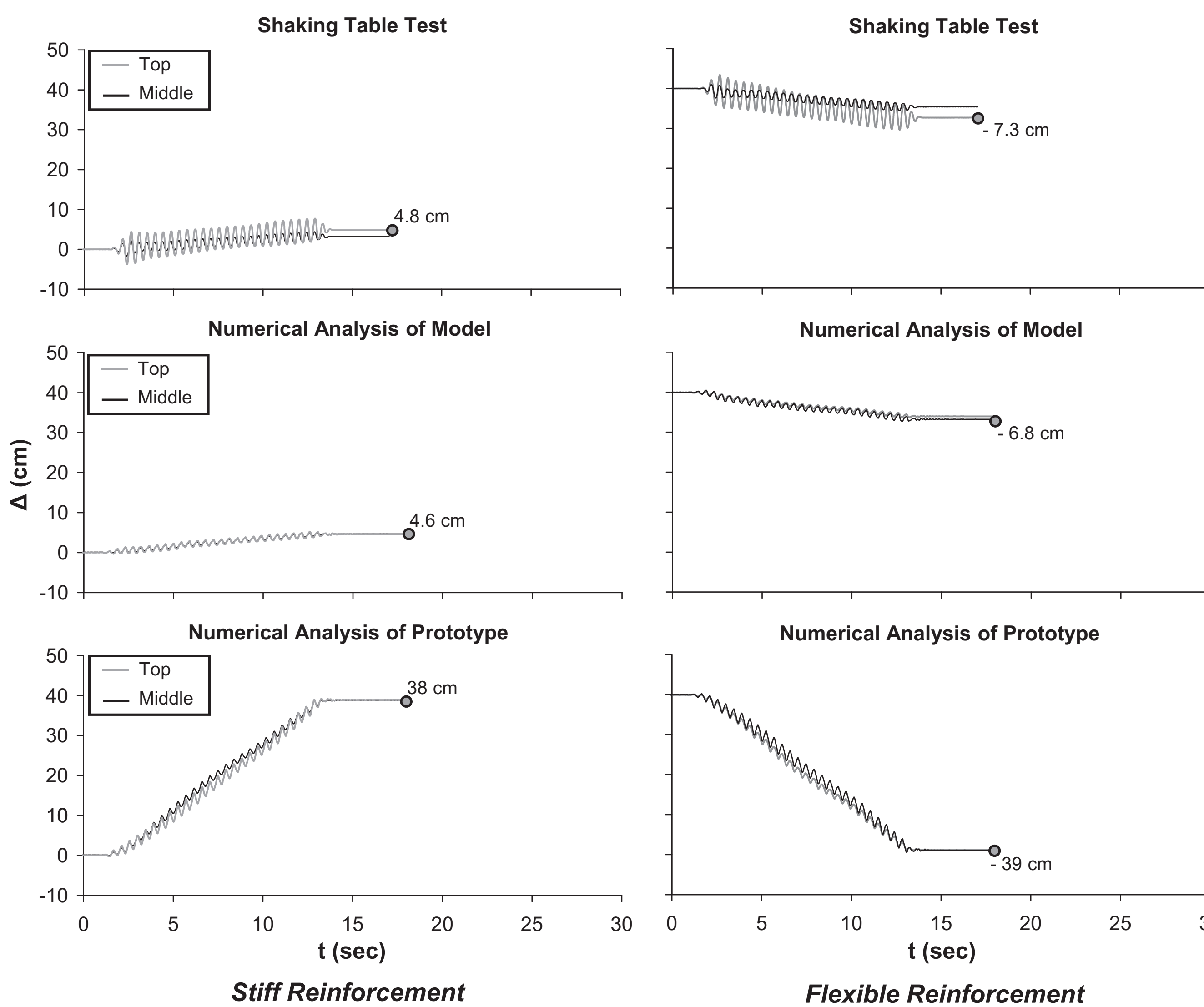

Fig. 18. Shaking table (top row) versus numerical analysis (middle and bottom row): modeling the test with soil properties as measured for low confining pressures (middle row); modeling the prototype with soil properties appropriate for realistic confining pressures (bottom row). Wall displacement time histories for the multi-cycle seismic excitation of $T=0.4$ s (results shown in prototype scale).

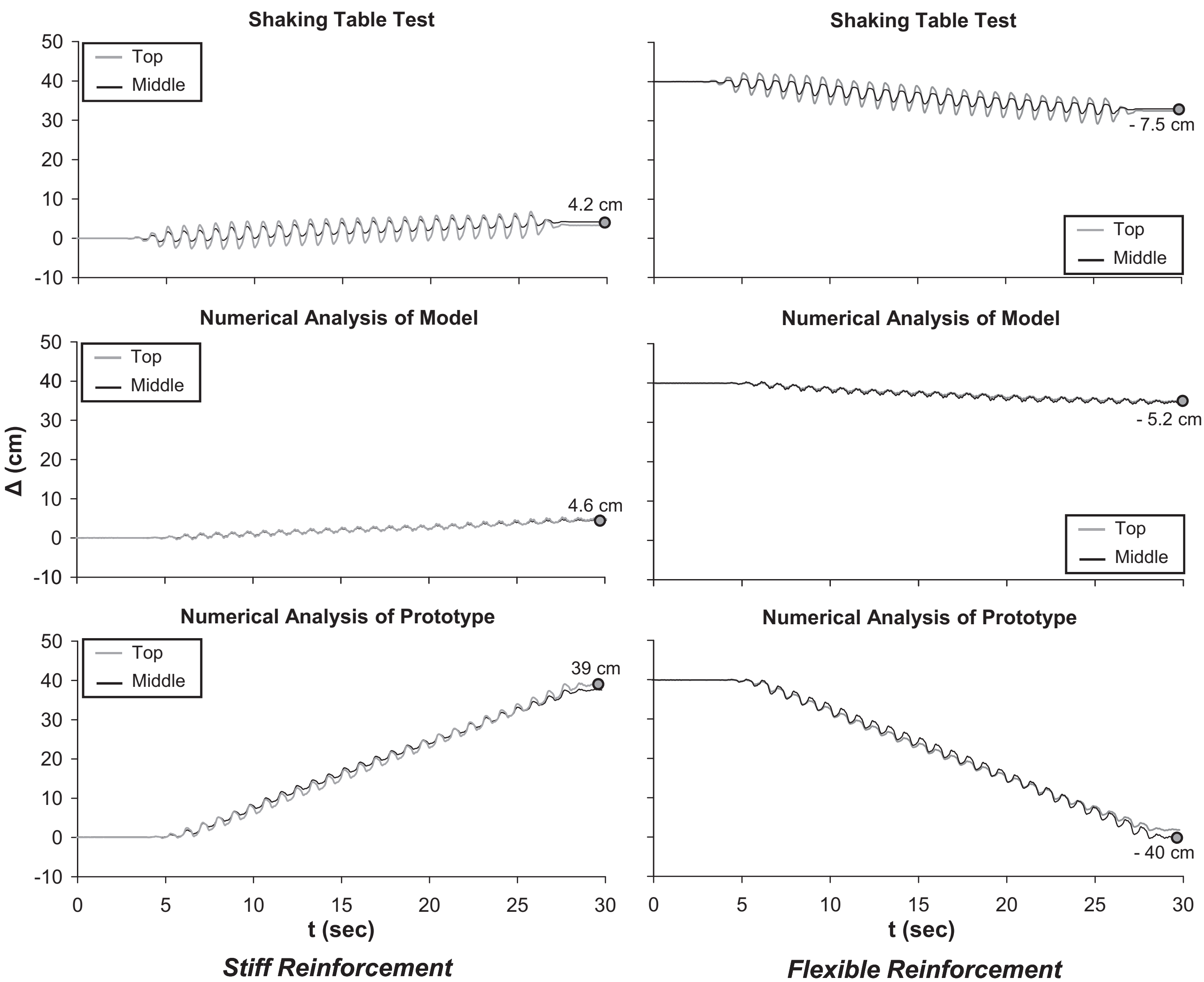

Fig. 19. Shaking table (top row) versus numerical analysis (middle and bottom row): modeling the test with soil properties as measured for low confining pressures (middle row); modeling the prototype with soil properties appropriate for realistic confining pressures (bottom row). Wall displacement time histories for the multi-cycle seismic excitation of $T=0.8$ s (results shown in prototype scale).

Table 3
Summary comparison of numerical analysis with shaking table test results: maximum permanent horizontal wall displacements.

	Shaking table test		Numerical analysis			
			Shaking table model		Extrapolation to prototype	
	Wall A (cm)	Wall B (cm)	Wall A (cm)	Wall B (cm)	Wall A (cm)	Wall B (cm)
Kalamata 1986	1.1	0.5	0.8	0.8	1.3	2.1
Lefkada 1973	1.9	1.5	1.2	0.1	2.9	1.0
Lefkada 2003	2.0	3.7	4.7	4.8	12.6	11.7
Rinaldi 228	9.3	2.5	9.7	4.6	16.6	8.1
Cos sweep $T=0.4$ s	4.8	7.3	4.6	6.8	38.1	38.9
Cos sweep $T=0.8$ s	4.2	7.5	4.6	5.2	38.7	39.6

Wall A: "*stiff*" reinforcement.
Wall B: "*flexible*" reinforcement.

component of the horizontal (lateral) wall displacement, but the residual displacement (the key performance indicator of retaining systems) is in line with the experimental results for all cases examined herein (reinforcement stiffness and dominant period of the seismic motion). As summarized in Table 3, the same conclusion is generally valid for real records. But with some

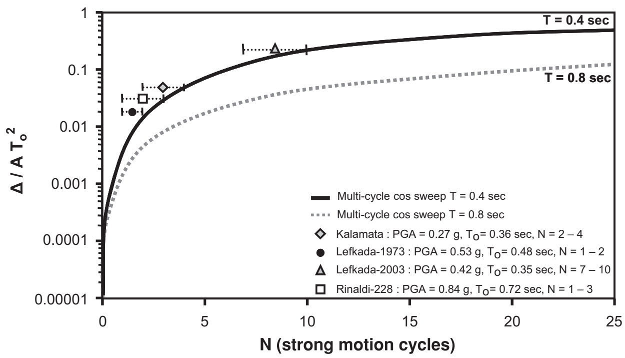

Fig. 20. Synopsis of numerical results recast in dimensionless form for the prototype (i.e. with soil properties appropriate for typical realistic confining pressures): normalized residual wall displacement Δ/AT_2^0 with respect to the number of strong-motion cycles *N*.

exceptions: the Lefkada 2003 test results for wall A are quite lower than the numerical prediction (2 cm versus 4.7 cm). But despite such discrepancies the performance of the numerical model is quite satisfactory—especially in view of the fact that the various motions were applied consecutively (one after the other) in the shaking table test; this was not done in the analysis.

We thus may proceed with some confidence to the numerical prediction of prototype performance (an indirect extrapolation to prototype scale). A first, expected, conclusion is that all permanent wall displacements are larger in prototype scale (Table 3): with $\varphi = 38^\circ$ (for the *high* confining pressures of the prototype) instead of 58^o (for the *small* confining pressures of the shaking table test), the "sliding" displacements can only become larger. The differences between model and prototype are not that pronounced for seismic motions of moderate intensity (Kalamata, Lefkada-1973). The discrepancies become larger for Lefkada-2003, which has about 8 strong motion cycles: the 5 cm of residual horizontal displacement of the test become more than 12 cm for the prototype. Even larger are the differences for the 30-cycle cos-sweeps (see also Figs. 18 and 19): while Δ ranges from 5 to 7 cm in the case of the shaking table test, it becomes 38–40 cm for the prototype. Interestingly, the differences are not so pronounced for the Rinaldi record: 16 cm instead of 9 cm for the shaking table test. In summary, the discrepancies between model and prototype (due to the unavoidable role of scale effects) seem to become larger with the increase of strong motion cycles (i.e. with the accumulation of "sliding" displacements).

Fig. 20 summarizes the performance of the prototype in terms of non-dimensional permanent wall displacement Δ/AT_o^2 (where A=PGA, and T_o=dominant period of the motion) with respect to the number *N* of equivalent strong motion cycles. The results of real records are plotted in an approximate manner, after some reasonable assumptions concerning their *A*, T_o, and *N*. Observe that Δ/AT_o^2 is substantially larger for the T_o=0.4 s cos-sweep compared to the longer period one (T_o=0.8 s), something which can be attributed to differences in terms of dynamic response (larger amplification in the first case). Additionally, the non-dimensional displacement of real records (at least of the ones tested and analyzed here) falls quite close to that of the T_o=0.4 s cos-sweep, implying a more general validity of this non-dimensional diagram.

6. Summary and conclusions

This paper has investigated *experimentally and numerically* the seismic performance of typical bar-mat-reinforced soil retaining walls. The main conclusions of the work presented herein are as follows:

[1] Although the stress field in the backfill soil cannot be correctly reproduced in reduced-scale shaking table testing, the latter can be used to simulate the behavior of reinforced soil walls, provided that the results are interpreted carefully, with due consideration to scale effects and the stress dependent soil behavior. A combined experimental-numerical methodology has been employed to indirectly "extrapolate" the results of shaking table testing to prototype conditions.

[2] For this purpose, a modified kinematic hardening model was developed and encoded in the finite element code through a user subroutine. After calibrating model parameters through laboratory element testing, the retaining walls were analyzed at model scale, assuming soil parameters for small confining pressures. After validating the numerical method the problem was analyzed at prototype scale assuming soil parameters for standard confining pressures. Thus, the results of shaking table testing were indirectly "converted" to real scale.

[3] The lateral displacement of the reinforced soil wall consists of two components: a cyclic (oscillatory) component, and a permanent (cumulative) component. The former is related to the elastic inertial response of the system, while the latter can be seen as the result of accumulation of "sliding" displacement of the reinforced soil block along its corresponding active failure wedge.

[4] For small to medium intensity seismic motions, typical of $M_s \approx 6.0$ earthquakes at relatively small distance from the fault, the response of the reinforced soil walls is "*quasi-elastic*". Permanent lateral displacements do not exceed a few centimeters (at prototype scale), and the associated settlement is rather minor.

[5] For larger intensity seismic motions, typical of $M_s \approx 6.5$–7.0 earthquakes near the seismogenic fault, bearing the influence of forward rupture directivity or having a large number of strong motion cycles, plastic deformation takes place and an active failure wedge behind the reinforced soil area starts forming, but cannot develop completely. Permanent lateral displacement of the bar-mat is of the order 10–15 cm (at prototype scale), which can be characterized as totally acceptable for this type of shaking.

[6] A large number of strong motion cycles ($N > 30$) of *unrealistically* large amplitude (A=1.0 g) is required for the active failure wedge behind the reinforced soil block to develop completely. Only under such *unrealistic* conditions, can a conservatively designed reinforced soil wall reach its ultimate capacity. In such a case, the permanent lateral displacements may be excessively large.

[7] Overall, it could be argued that the seismic performance of the bar-mat-reinforced soil walls investigated in this paper is quite acceptable for realistic levels of seismic excitation.

Acknowledgements

This work forms part of an EU 7th Framework research project funded through the European Research Council's Programme "Ideas", Support for Frontier Research—Advanced Grant under Contract number ERC-2008-AdG228254-DARE to Professor G. Gazetas. The authors gratefully acknowledge the encouragement and guidance of Professor Gazetas throughout this research effort.

References

[1] Gazetas G, Psarropoulos P, Anastasopoulos I, Gerolymos N. Seismic behaviour of flexible retaining systems subjected to short duration moderately strong excitation. Soil Dynamics & Earthquake Engineering 2004;24(7):537–50.

[2] Frankenberger PC, Bloomfield RA, Anderson PL, 1996. Reinforced Erath Walls Withstand Northridge Earthquake, Earth Reinforcement, Ochiai, Balkema, Rotterdam, Isbn: 90-5410-833-9.

[3] Earthquake Engineering Research Institute, 1995, The Hyogo-Ken Nanbu earthquake, January 17, 1995, Preliminary EERI Reconnaissance Report, 1995.

[4] Committee of Earthquake Engineering. The 1995 Hyogo-Ken Nanbu earthquake—investigation into damage to civil engineer structures, Japan Society of Civil Engineers 1996.

[5] Japanese Geotechnical Society. Geotechnical aspects of the January 17, 1995 Hyogoken-Nambu earthquake. Soils and Foundations, Special Issue 1996. January 1996.

[6] Seible F, Priestley MJN, MacRae G. The Kobe earthquake of January 17, 1995; initial impressions from a quick reconnaissance, Structural systems research report-95/03. University of California, San Diego; 1995.

[7] Tatsuoka F, Tateyama M, Koseki J. Performance of soil retaining walls for railway embankments. Soils and Foundations, Special Issue on Geotechnical Aspects of the January 17 1995 Hyogoken-Nanbu Earthquake 1996;1:311–24.

[8] Tatsuoka F, Koseki J, Tateyama M. Performance of reinforced soil structures during the 1995 Hyogo-ken Nambu Earthquake. In: Ochiai, Yasufuku, Omine, editors. Earth reinforcement, vol. 2; 1997. p. 979–1008.

[9] Koseki J, Tatsuoka F, Munaf Y, Tateyama M, Kojima K. A modified procedure to evaluate active earth pressure at high seismic loads. Soils and Foundations, Special Issue on Geotechnical Aspects of the January 17 1995 Hyogoken-Nambu Earthquake 1998;2:209–216.

[10] Koseki J. Seismic performance of retaining walls-case histories and model tests. Proceedings of the fourth forum on implications of recent earthquakes on seismic risk. Japan: Tokyo Institute of Technology; 2002. 95–107.

[11] Kobayashi K, Tabata H, Boyd M. The performance of reinforced earth structures in the vicinity of Kobe during the Great Hanshin Earthquake, Earth Reinforcement, Ochaia, Balkema Rotterdam; 1996. Isbn: 90-5410-833-9.

[12] Tatsuoka F, Koseki J, Tateyama M, Munaf Y, Horii K. Seismic stability against high seismic loads of geosynthetic reinforced soil retaining structures. Proceedings of the sixth international conference on geosynthetics, vol. 1; 1998. p. 103–141.

[13] Michalowski RL, Čermák J. Triaxial compression of sand reinforced with fibersJournal of the Geotechnical Engineering Division, ASCE 2003;192(2):125–136.

[14] Zornberg JG, Sitar N, Mitchell JK. Performance of geosynthetic reinforced slopes at failure. Journal of the Geotechnical Engineering Division 1998;124(8):670–83.

[15] Takahashi A, Takemura J, Izawa J. Dynamic behavior of vertical geogrid-reinforced soil during earthquake. Proceedings of the international symposium on slope stability engineering, vol. 2; 1999. p. 991–996.

[16] Zornberg JG, Arriaga F. Strain distribution within geosynthetic-reinforced slopesJournal of Geotechnical and Geoenvironmental Engineering, ASCE 2003;129(1):32–45.

[17] Ichikawa S, Suemasa N, Katada T, Toyosawa Y. Centrifuge model tests on seismic stability of reinforced retaining wall. The fifth workshop on safety & stability of infrastructures against environmental impacts. 2005. CD-ROM.

[18] Ling HI, Liu H, Kaliakin VN, Leshchinsky D. Analyzing dynamic behavior of geosynthetic-reinforced soil retaining wallsJournal of Engineering Mechanics, ASCE 2004;130(8):911–920.

[19] Siddharthan RV, Ganeshwara V, Kutter BL, El-Desouky M, Whitman RV. Seismic deformation of bar mat mechanically stabilized earth walls—centrifuge tests. Journal of Geotechnical and Geoenvironmental Engineering 2004;130(1):14–25.

[20] Ishihama Y, Izawa J, Kuwano J. Centrifuge tilting and shaking table tests on the RSW with different soils. Proceedings of the third Asian regional conference on geosynthetics (GeoAsia 2004). 2004. p. 803–810.

[21] Nova-Roessig L, Sitar N. Centrifuge model studies of the seismic response of reinforced soil slopesJournal of Geotechnical and Geoenvironmental Engineering, ASCE 2006;132(3):388–400.

[22] Ramakrishnan K, Budhu M, Britto A. Laboratory seismic tests on geotextile wrap-faced and geotextile-reinforced segmental retaining walls. Geosynthetics International 1998;5(1–2):55–71.

[23] Koseki J, Kato N, Watanabe K, Tateyama M. Evaluation of Seismic Displacement of Reinforced Walls. Proceeding of the 3rd Asian Regional Conference on Geosynthetics (GeoAsia 2004). 2004. p. 217–224.

[24] Bathurst RJ, Walters D, Vlachopoulos N, Burgess P, Allen TM. Full scale testing of geosynthetic reinforced walls. Proceedings of GeoDenver 2000. Denver, Colorado: ASCE Special Publication; 2000 p. 1–17.

[25] Burke C, Ling HI, Liu H. Seismic response analysis of a full-scale reinforced soil retaining wall. 17th ASCE Engineering Mechanics Conference. 2004.

[26] Ling HI, Mohri Y, Leshchinsky D, Burke C, Matsushima K, Liu H. Large-scale shaking table tests on modular-block reinforced soil retaining wall. Journal of Geotechnical and Geoenvironmental Engineering 2005;131(4):465–76.

[27] Koseki J, Munaf Y, Tatsuoka F, Tateyama M, Kojima K, Sato T. Shaking and tilt table tests of geosynthetic-reinforced soil and conventional-type retaining walls. Geosynthetics International 1998;5(1–2):73–96.

[28] Gibson, AD. Physical scale modeling of geotechnical structures at One-G, Report no. SML 97-01. Pasadena, CA: California Institute of Technology; 1997. p. 413.

[29] Kolbuszewski J. An experimental study of the maximum and minimum porosities of sandsProceedings of the second ICSMFE, vol. 1; pp. 158–165.

[30] Georgiannou VN, Tsomokos A, Stavrou K. Monotonic and cyclic behaviour of sand under torsional loading. Géotechnique 2008;58(2):113–24.

[31] Hight DW, Gens A, De Campos TMP, Takahashi M. Factors influencing the interpretation of in situ strength tests in insensitive low plasticity clays. Proceedings of International Conference Behaviour of Off-Shore Structures 1983 pp. 438–450.

[32] Louvari E, Kiratzi AA, Papazachos BC. The cephalonia transform fault and its extension to western Lefkada Island (Greece). Tectonophysics 1999;308:223–36.

[33] Gazetas G, Dakoulas P, Papageorgiou AS. Local soil and source mechanism effects in the 1986 Kalamata (Greece) earthquake. Earthquake Engineering & Structural Dynamics 1990;19:431–56.

[34] Kramer SL, Lindwall NW. Dimensionality and directionality effects of newmark stability analysis. Journal of Geotechnical and Geoenvironmental Engineering, ASCE 2004;130:303–15.

[35] Fardis N, Georgarakos P, Gazetas G, Anastasopoulos I. Sliding isolation of structures: effect of horizontal and vertical acceleration. Proceedings of the FIB International Symposium on "Concrete Structures in Seismic Regions". 2003. in CD-Rom.

[36] Garini E, Gazetas G, Anastasopoulos I. Accumulated asymmetric slip caused by motions containing severe 'directivity' and 'fling' pulses, Géotechnique 2010, in press.

[37] Benetatos C, Kiratzi A, Roumelioti Z, Stavrakakis G, Drakatos G, Latoussakis I. The 14 August 2003 Lefkada Island (Greece) earthquake: focal mechanisms of the mainshock and of the aftershock sequence. Journal of Seismology 2005;9(2):171–90.

[38] Gazetas G, Anastasopoulos I, Dakoulas P. Failure of harbor quaywall in the Lefkada 2003 earthquake. Proceedings of geotechnical earthquake engineering satellite conference—performance based design in earthquake geotechnical engineering: concepts and research. 2005. p. 62–69.

[39] Trifunac MD, Todorovska MI, Lee VW. The Rinaldi strong motion accelerogram of the Northridge, California, earthquake of 17 January, 1994. Earthquake Spectra 1998;14(1):225–39.

[40] Somerville P. Seismic hazard evaluation. Bulletin of the N. Zealand Society for Earthquake Engineering 2000;33(3):371–86. No. 4, p. 484–491..

[41] ABAQUS, Inc., 2008. ABAQUS user's manual, Providence, R.I.

[42] Ishibashi I, Zhang X. Unified dynamic shear moduli and damping ratios of sand and clay. Soils and Foundations 1993;33(1):12–191.

[43] Seed HB, Wong RT, Idriss IM, Tokimatsu K. Moduli and damping factors for dynamic analyses of cohesionless soils. Journal of Geotechnical Engineering, ASCE 1986;112(11):1016–32.

[44] Hardin BO, Richart FE. Elastic wave velocities in granular soils. Journal of the Soil Mechanics Foundations Divsion, ASCE 1963;89(SM1):33–65.

[45] Cole Jr. DA, Lade PV. Influence zones in alluvium over dip-slip faults. Journal of Geotechnical Engineering, ASCE 1984;110(5):599–615.